Journal of Hazardous Materials 211–212 (2012) 233–239

Contents lists available at SciVerse ScienceDirect

Journal of Hazardous Materials

journal homepage: www.elsevier.com/locate/jhazmat

Adsorption and photocatalytic oxidation of formaldehyde on a clay-TiO_2 composite

Daria Kibanova[a,b], Mohamad Sleiman[c], Javiera Cervini-Silva[b,d,**], Hugo Destaillats[c,e,*]

[a] Facultad de Química, Universidad Nacional Autónoma de México, Mexico
[b] Departamento de Procesos y Tecnología, Universidad Autónoma Metropolitana, Mexico
[c] Lawrence Berkeley National Laboratory, Indoor Environment Group, Environmental Energy Technologies Division, USA
[d] NASA Astrobiology Institute, USA
[e] Arizona State University, Department of Chemistry and Biochemistry, USA

ARTICLE INFO

Article history:
Received 11 August 2011
Received in revised form
30 November 2011
Accepted 1 December 2011
Available online 17 December 2011

Keywords:
P25
Clay
Hectorite
Photocatalyst
Aldehyde
Relative humidity

ABSTRACT

We investigated the adsorption capacity and photocatalytic removal efficiency of formaldehyde using a hectorite-TiO_2 composite in a bench flow reactor. The same experimental conditions were applied to pure TiO_2 (Degussa P25) as a reference. The catalysts were irradiated with either a UVA lamp (365 nm) or with one of two UVC lamps of 254 nm and 254 + 185 nm, respectively. Formaldehyde was introduced upstream at concentrations of 100–500 ppb, with relative humidity (RH) in the range 0–66% and residence times between 50 and 500 ms. Under dry air and without illumination, saturation of catalyst surfaces was achieved after ~200 min for P25 and ~1000 min for hectorite-TiO_2. The formaldehyde uptake capacity by hectorite-TiO_2 was 4.1 times higher than that of P25, almost twice the BET surface area ratio. In the presence of humidity, the difference in uptake efficiency between both materials disappeared, and saturation was achieved faster (after ~200 min at 10% RH and ~60 min at 65% RH). Under irradiation with each of the three UV sources, removal efficiencies were proportional to the Ti content and increased with contact time. The removal efficiency decreased at high RH. A more complete elimination of formaldehyde was observed with the 254 + 185 nm UV source.

Published by Elsevier B.V.

1. Introduction

Formaldehyde (HCHO) is an ubiquitous indoor pollutant released from wood-based building products and furnishings, among other natural and anthropogenic sources [1]. Formaldehyde forms as a result of the oxidation of volatile organic compounds (VOCs) by either ozone or hydroxyl ($OH^{\bullet}$) radicals under atmospheric conditions [2,3]. Indoor exposure to HCHO is associated with increased risks of asthma and allergy [4]. Reportedly, observed changes in nasal lavage fluids during formaldehyde inhalation have been attributed to non-specific proinflammatory properties [5]. Asthma and allergies are reported to affect ca. 6% and 20% of the 89 million US workers in nonagricultural and nonindustrial indoor settings, respectively. Such health consequences stemming from formaldehyde inhalation in the workplace has been reported to cause productivity losses ranging from 20 to 70$B yr^{-1} [6]. Furthermore, formaldehyde is listed by USEPA as a probable carcinogen (group B1, USEPA), and the World Health Organization has classified formaldehyde as a human carcinogen [7]. Surveys conducted in both US commercial buildings and homes showed mean indoor HCHO concentrations values ca. 11 and 17 ppbv, respectively. Such concentrations are higher than the 8-h reference exposure levels proposed by the California Environmental Protection Agency, i.e., 7 ppbv, and are close to the 8-h recommended level for occupational exposure in the US (16 ppbv) [8]. Current indoor-air pollutant exposure scenarios are likely to worsen in a near future provided that adaptation to climate change and urban heat island effects may lead to increases in the use of air conditioning, tighter building envelopes, as well as to lower air-exchange rates [9]. In addition, expanding urbanization and changes in land use patterns may contribute to increased surface-level concentrations of ozone, an indoor formaldehyde precursor [10].

Advanced indoor air cleaning technologies can play an important role in mitigating indoor exposures. In a related work we have tested prototype TiO_2 photocatalytic oxidation (PCO) air cleaners.

* Corresponding author at: Lawrence Berkeley National Laboratory, 1 Cyclotron Road, MS 70-108B, Berkeley, CA 94720, USA. Tel.: +1 510 486 5897; fax: +1 510 486 7303.
** Corresponding author at: Departamento de Procesos y Tecnología, División de Ciencias Naturales e Ingeniería, Universidad Autónoma Metropolitana, Unidad Cuajimalpa (UAM-C), Artificios No. 40, 6° Piso, Col. Miguel, Hidalgo, Delegación Álvaro Obregón, C.P. 01120, México, D.F., Mexico. Tel.: +52 55 26 36 38 00x3827; fax: +52 55 26 36 38 00x3832.
E-mail addresses: jcervini@correo.cua.uam.mx (J. Cervini-Silva), HDestaillats@lbl.gov (H. Destaillats).

0304-3894/$ – see front matter. Published by Elsevier B.V.
doi:10.1016/j.jhazmat.2011.12.008

Table 1
Preparation of photocatalyst-coated Raschig rings.

Material	m_f (mg)	TiO_2 content[a] (%)	$m_{f\text{-}TiO_2}$ (mg)	BET surface area[a] ($m^2\,g^{-1}$)	Average pore volume[a] ($cm^3\,g^{-1}$)
Hecto-TiO_2	1.03	60.8	0.626	140	0.457
P25	0.762	100	0.762	60.7	0.308

[a] Data taken from Ref. [14].

The results have showed promise in the simultaneous abatement of VOCs present in multi-component mixtures at typical indoor levels [11–13]. We observed single-pass conversion efficiencies better than 20% for most VOCs, reaching in some cases as much as 80% removal. Although volatile aldehydes can be eliminated by PCO at rates comparable to those for other VOCs, incomplete mineralization of a few target compounds present in the mixtures (alcohols, terpenes) results in the formation of additional HCHO, acetaldehyde, and other partially oxidized byproducts. For the experimental conditions tested, HCHO outlet/inlet concentration ratios were between 1.9 and 7.2. Given the data variability observed, it becomes clear the need for improving experimental conditions towards PCO applications.

Clay-TiO_2 nanocomposites have been postulated as suitable alternative photocatalysts in environmental applications. In particular, for air treatment considerations, these materials offer a large porous structure for VOC adsorption and high adsorption capacity. Recently, we have synthesized hectorite-TiO_2 composite (hecto-TiO_2) [14], a titania-rich material (60% TiO_2) with significantly higher BET surface than Degussa P25 TiO_2 ($BET_{hecto-TiO_2}/BET_{P25} = 2.3$). We tested the material towards toluene as probe compound. When challenged with toluene vapor, hecto-TiO_2 showed a performance comparable to P25 under air either under dry conditions or low relative humidity, ca. ≤10% RH. However, hecto-TiO_2 performance was found to become partially inhibited at higher humidity, ca. 33% and 66% RH [15]. These findings were explained as the consequence of water adsorption and condensation at nano-sized pores sites, which limits the access of hydrophobic compound molecules to TiO_2 active sites. In this study, we challenge hecto-TiO_2 under similar testing conditions with HCHO, a hydrophilic compound. The purpose is to explore the photocatalytic activity of surface clay-TiO_2 composites towards HCHO, and better understand the effect of water co-adsorption in photocatalytic efficiency.

2. Experimental

2.1. Preparation of clay-supported TiO_2

Hectorite ($Na_{0.4}Mg_{2.7}Li_{0.3}Si_4O_{10}(OH)_2$; SHCa-1) from San Bernardino County, CA, USA, was purchased from the Source Clays Repository of the Clay Minerals Society (West Lafeyette, IN), and used as received. A description of the synthesis and characterization of the TiO_2–clay nanocomposites has been reported previously [14]. Briefly, a 1% (w/w) clay–water suspension was stirred for 2 h. A TiO_2 sol–gel solution was prepared by mixing titanium tetraisopropoxide $Ti(OC_3H_7)_4$ (97%, Sigma–Aldrich, Milwaukee, WI) with hydrochloric acid (37%, reagent grade, Aldrich, Milwaukee, WI), de-ionized water (17.6 MΩ cm, Millipore) and absolute ethanol (≥98%, Riedel-de Haen, Switzerland). The concentration of $Ti(OC_3H_7)_4$ in the sol–gel solution (Solution A) was 0.4 M. The $H_2O/Ti(OC_3H_7)_4$ molar ratio for Solution A was adjusted to 0.82, and the pH was 1.27. Solution A was diluted with absolute ethanol to obtain a $Ti(OC_3H_7)_4$ concentration ca. 0.05 M (Solution B). An aliquot of Solution B was added to the clay suspension to adjust the TiO_2 content in suspension ca. 70% (w/w). The resulting suspension was stirred for 24 h, and then centrifuged at 3800 rpm for 10 min. The solid phase was recovered and washed three times with de-ionized water. The hectorite-TiO_2 composite was dispersed in a 1:1 water:ethanol solution, and then exposed to hydrothermal treatment at 180 °C for 5 h. The product was centrifuged once again at 3800 rpm for 15 min, and re-suspended in absolute ethanol (Solution C).

2.2. Preparation of photocatalyst-coated Raschig rings

Fifty Raschig glass rings (5 mm OD × 5 mm length; Ace Glass, Vineland, NJ) were coated with hecto-TiO_2 composite and fifty more were coated with P25 (TiO_2, Degussa, Germany). Before coating, the rings were initially sonicated for 5 min in acetone (J.T. Baker), and for 5 min in de-ionized water; and oven-dried at 60 °C for 1 h. Each ring was dip-coated for 5 s in suspensions containing (a) Solution C or (b) P25 suspended in ethanol. Coated rings were placed in an oven at 110 °C for 5 h to evaporate the solvent. Dried-coated rings were stored in ambient conditions prior to use.

The average mass of the photocatalytic material deposited in each ring was determined as follows:

$$m_f = \frac{(m_c - m_g)}{50} \quad (1)$$

where m_f is the average mass of photocatalytic material per ring; m_c is the mass of 50 coated rings; and m_g is the mass of the same 50 rings determined before coating. Shown in Table 1 are data for average mass (m_f), average mass of TiO_2 deposited per ring ($m_{f\text{-}TiO_2}$), as well as BET surface area for each catalyst, average pore area for hecto-TiO_2 and equivalent average pore area for P25, as determined by the BJH method.

2.3. Photocatalytic reactor and experimental methods

2.3.1. Photocatalytic reactor and UV lamps

The photocatalytic flow reactor used in the experiments has been described previously [15,16]. Briefly, the reactor consisted of a cylindrical-quartz tube containing a variable number of coated or uncoated-Raschig rings, which were irradiated by a UV-lamp and placed parallel to the tube at a constant distance ca. 25 mm. Three-different lamps were used: a UVA lamp with λ_{max} = 365 nm and irradiance I_{365} = 0.77 mW cm^{-2} (UVP Model 90-0019-01), a UVC lamp (UVC/O_3) with λ_{max} = 254 nm and secondary emission at 185 nm with an irradiance I_{254} = 2.8 mW cm^{-2} (UVP Model 90-0004-01) and a second UVC lamp (Spectroline Model 11SC-1 OF) with λ_{max} = 254 nm and an irradiance I_{254} = 4.45 mW cm^{-2}. The magnitude for the irradiance of the lamps at 25 mm from the source was determined with a UVP radiometer calibrated at 365 nm and 254 nm, respectively.

2.3.2. Formaldehyde source

Paraformaldehyde (J.T. Baker, Phillipsburg, NJ) was used to generate a constant flow of formaldehyde [17]. A constant airflow of "zero" quality air of 300 mL min^{-1} was circulated through the diffusion vial containing paraformaldehyde placed in a water bath at constant temperature (20 ± 1 °C). The generated formaldehyde concentration at the source outlet varied between 530 and 650 ppbv. A 100 mL min^{-1} flow was diverted from the source outlet and diluted with either dry or humid air. The flow and concentration of formaldehyde at the reactor inlet were adjusted to ca. f = 500 mL min^{-1} and $[HCHO]_{inlet}$ = 110–130 ppbv, respectively.

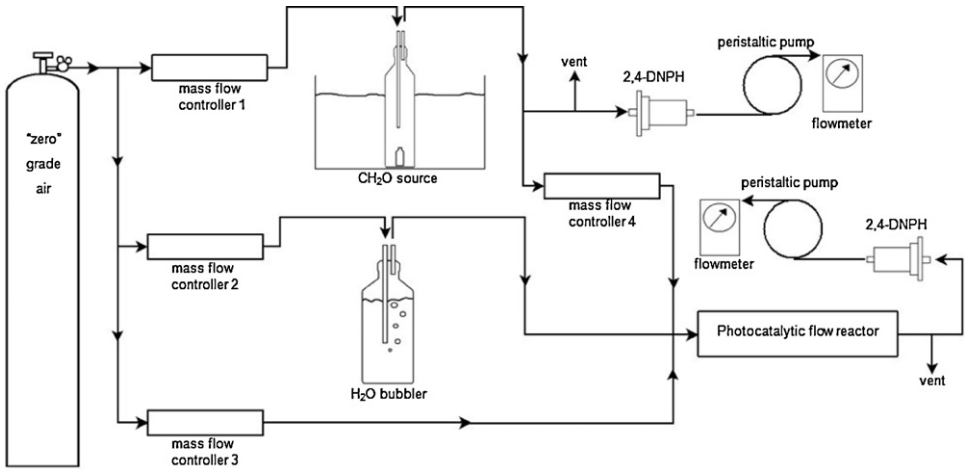

Fig. 1. Experimental setup.

For selected experiments the source inlet airflow was adjusted to 600 mL min^{-1} delivering 410–470 ppbv HCHO for dilution purposes with dry or humid air. The total flow and HCHO concentration were adjusted to f = 2 L min^{-1} and $[HCHO]_{inlet}$ = 75–80 ppbv, respectively.

2.3.3. Experimental setup and sampling procedures

The experimental setup is illustrated in Fig. 1. Three mass-airflow controllers (FC-280 TYLAN) were used in parallel to adjust the flow of "zero" quality air from a commercial cylinder (Airgas, California) with a precision ≤1%. One of the airflows carried HCHO as described above. The second airflow was saturated with moisture using a water bubbler. The third airflow contained dry air to adjust the relative humidity (RH) after mixing. All flow magnitude values were measured with a calibrated flowmeter (Dry Cal, BIOS Int.). Quantitation of RH was determined in real time at the reactor outlet using a HOBO sensor (Onset Corp., MA). Ozone concentrations were determined in real time at the reactor outlet using an ozone monitor (2B Technologies).

Formaldehyde samples were collected simultaneously at the source and at the reactor outlet for experiments in which the total flow was adjusted to f = 500 mL min^{-1}. Instead, when the total flow was f = 2 L min^{-1}, formaldehyde samples were collected successively from the reactor inlet and outlet. Samples were collected using 2,4-dinitrophenylhydrazine (DNPH)-coated silica cartridges (Waters, MA) preceded by a ozone scrubber (Waters, Milford, MA) for UVC/O_3 lamp experiments. DNPH cartridges were extracted with 2-mL acetonitrile (UV grade, Honeywell B&J, Muskegon, MI) and analyzed by HPLC (Agilent 1200 Series) with UV detection at 360 nm, in accordance with the US EPA Standard Method TO-11 [18].

For formaldehyde adsorption experiments a constant diluted formaldehyde flow (f = 500 mL min^{-1}) at different relative humidity (RH) levels was circulated through the reactor, and HCHO samples were collected at the inlet and outlet with t = 0 determined by the initial connection of the HCHO to the reactor.

Formaldehyde photocatalytic removal experiments were carried out by irradiating the rings (coated with P25, hecto-TiO_2 or uncoated rings) with UV light (UVA, UVC or UVC/O_3) at 0%, 10%, and 65% RH. In all experiments, diluted formaldehyde was allowed to circulate through the reactor without UV irradiation, in order to reach equilibrium with the photocatalyst and the other reactor internal surfaces. At equilibrium, the existing difference between HCHO-inlet and outlet concentrations approached zero. Then, the UV light was turned on for ca. 30 min prior to sample collection.

For experiments evaluating the effect of the residence time, only the UVA lamp was used, and the relative humidity was adjusted at 10%. For long-residence time experiments, 7 photocatalyst-coated rings were irradiated using a total flow of f = 500 mL min^{-1}. For mid-residence time experiments, a similar number of rings and a total flow of f = 2 L min^{-1} was selected. For short-residence time experiments, 3 photocatalyst-coated rings were irradiated and a total flow of f = 2 L min^{-1} was used.

3. Results and discussion

3.1. Formaldehyde adsorption in the absence of illumination

We studied the adsorption of HCHO to each of the photocatalysts in the dark, at different humidity conditions. These tests allowed us to determine the minimum time needed to complete HCHO uptake and saturation of the photocatalyst surface, in order to perform subsequent experiments by irradiating with UV light. Equilibrium saturation was reached when similar HCHO concentrations were measured simultaneously at the reactor inlet and outlet. As shown in Fig. 2 for experiments conducted with dry air, in the case of P25 saturation of the surface was reached at $t \sim 200$ min, after which adsorption of HCHO ceased. However, in the case of hecto-TiO_2 HCHO uptake continued until $t \sim 1000$ min. These saturation times for HCHO are significantly longer than those recorded for toluene under identical experimental conditions on our previous study (t < 30 min of equilibration [15]), suggesting that the chemical interactions between the catalyst and formaldehyde are of a very different nature with respect to those between the catalyst and hydrophobic hydrocarbons.

In Fig. 2, we plot HCHO uptake efficiency (%U) as a function of time, defined as

$$\%U = \left(1 - \frac{[HCHO]_{down}}{[HCHO]_{up}}\right) \times 100 \quad (2)$$

where $[HCHO]_{down}$ and $[HCHO]_{up}$ are the formaldehyde downstream and upstream concentrations, respectively. The area under the curves shown in Fig. 2 corresponds to the formaldehyde uptake capacity of each material. For dry air (0% RH), the uptake capacity was estimated to be 4.0 and 16.3 μg for P25 and hecto-TiO_2 respectively, by fitting a biexponential decay of each of the curves shown in Fig. 2. The ratio hecto-TiO_2/P25 of the area under both curves for results with dry air was estimated to be 4.1, significantly higher than the ratio of BET surface area determined for hecto-TiO_2 and P25 (equal to 140 m^2 g^{-1}/60.7 m^2 g^{-1} = 2.3). This difference

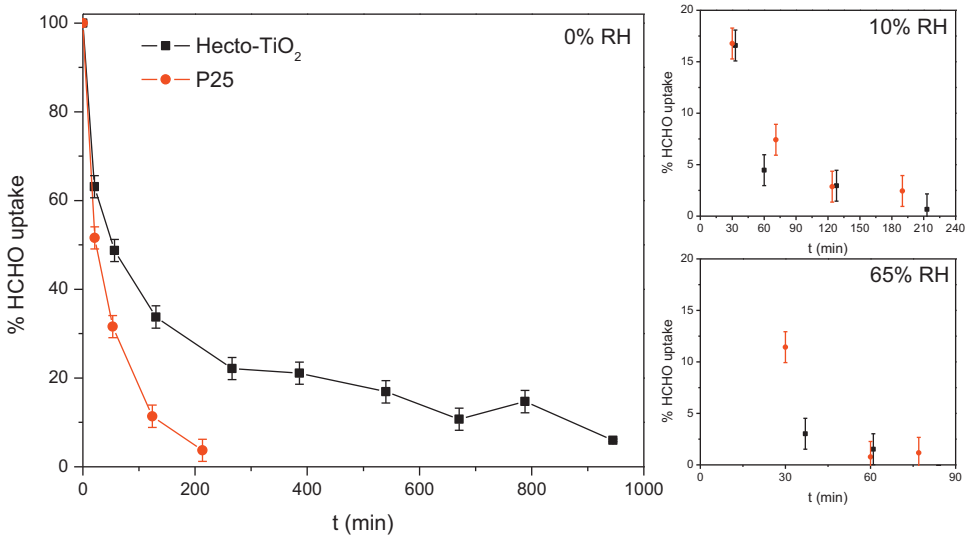

Fig. 2. Formaldehyde adsorption isotherms under dry air (0% RH), 10% RH and 65% RH.

suggests that the clay matrix has a higher intrinsic affinity for HCHO leading to higher uptake than what can be predicted solely on the basis of effective surface area of each material.

Fig. 2 also shows that at 10% and 65% RH the saturation equilibrium is achieved very fast in both cases, with imperceptible differences between P25 and the clay-TiO_2 composite. Furthermore, apparent saturation is achieved faster ($t \sim 60$ min) for experiments carried out at higher humidity (65% RH), vis-à-vis those carried out at 10% RH (saturation at $t > 120$ min). This experimental evidence highlights the critical role played by layers of adsorbed water on the catalyst surface. Due to catalyst pore water saturation, we assume that HCHO adsorption is lower for both catalysts under humidified air, compared to a similar scenario at 0% RH. Water and HCHO compete for adsorption and uptake. Adventitious water also limits diffusion of HCHO into the catalyst pores. Particularly, hecto-TiO_2 was found to show a very high water uptake with respect to P25 [15]. Our method did not allow us to explore other mechanisms potentially at play, such as different swelling behavior of the catalysts and water–formaldehyde chemical equilibria potentially leading to enhanced uptake.

3.2. Photocatalytic degradation under UV irradiation

Once the catalyst surface was saturated with formaldehyde, the UV lamp was turned on and we followed changes in concentrations at both ends of the reactor. Under UV irradiation, we determined the steady-state formaldehyde removal efficiency (%R) as a function of the upstream and downstream HCHO concentrations, as follows:

$$\%R = \left(1 - \frac{[\mathrm{HCHO}]_{\mathrm{down}}}{[\mathrm{HCHO}]_{\mathrm{up}}}\right) \times 100 \quad (3)$$

In experiments performed at a total flow rate of $f = 500$ mL min^{-1}, upstream HCHO concentrations were determined as the level measured at the source multiplied by a dilution factor corresponding to the ratio between the flow containing HCHO from the source and the total airflow being introduced into the reactor. For experiments carried out at $f = 2$ L min^{-1}, both HCHO concentrations were determined directly at the reactor outlet (with the UV lamp on or off), without applying any correction factor.

The formaldehyde removal rate F_r, expressed in ng min^{-1} was calculated as follows:

$$F_r = ([\mathrm{HCHO}]_{\mathrm{up}} - [\mathrm{HCHO}]_{\mathrm{down}}) \times f \quad (4)$$

where f is the airflow rate circulating through the reactor, expressed in mL min^{-1}. Table 2 summarizes the removal rates determined under three different illumination conditions and three different relative humidity settings, for each of the two catalysts studied. In all cases, formaldehyde removal due to UV irradiation in the absence of catalyst (blank) was subtracted. Blank removal efficiencies were ~6% for UVA and between 20% and 40% under UVC irradiation.

3.2.1. Effect of relative humidity

HCHO removal over all humidity conditions tested was found relatively higher in the case of P25 (Fig. 3). As shown in Table 2, HCHO removal rate normalized per TiO_2 content are similar for both materials at 0% RH. Our previous study [15] indicated that the TiO_2 content appears to be the driving parameter of the photocatalytic process, at 0% RH. We had also reported that at RH = 10%, P25 and hecto-TiO_2 exhibited maximum photocatalytic activity for toluene removal. By contrast, in the present case for HCHO, P25

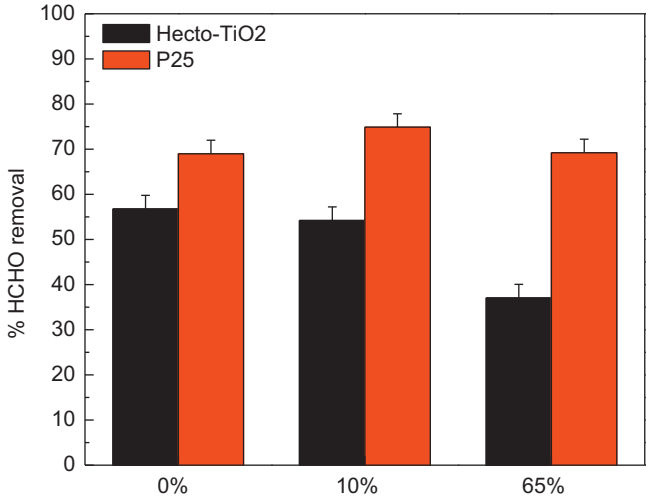

Fig. 3. Effect of relative humidity on HCHO photocatalytic removal under UVA irradiation.

Table 2
Formaldehyde photocatalytic oxidation under either UVA, UVC, or UVC/O_3 at $0 \leq RH \leq 65\%$.

RH	UVA			UVC			UVC/O_3		
	F_r (ng min^{-1})	F_r/m_f (ng min^{-1} g^{-1})	$F_r/m_{f\text{-}TiO_2}$ (ng min^{-1} g^{-1})	F_r (ng min^{-1})	F_r/m_f (ng min^{-1} g^{-1})	$F_r/m_{f\text{-}TiO_2}$ (ng min^{-1} g^{-1})	F_r (ng min^{-1})	F_r/m_f (ng min^{-1} g^{-1})	$F_r/m_{f\text{-}TiO_2}$ (ng min^{-1} g^{-1})
P25									
0	59.8	11.2	11.2	64.4	12.1	12.1	55.2	10.4	10.4
10	60.2	11.3	11.3	67.6	12.7	12.7	73.8	13.8	13.8
65	59.7	11.2	11.2	52.7	9.9	9.9	63.6	11.9	11.9
Hecto-TiO_2									
0	44.8	6.2	10.2	44.3	6.2	10.1	52.9	7.3	12.1
10	43.2	6.0	9.9	50.2	7.0	11.4	67.8	9.4	15.5
65	31.0	4.3	7.1	32.0	4.4	7.3	42.5	5.9	9.7

performance was still higher at 10% RH; however hecto-TiO_2 photocatalytic activity at 10% RH for HCHO removal was lower than in absence of H_2O. Finally, working at higher relative humidity of 65% partially inhibited hecto-TiO_2 performance, and P25 only to a minor extent. The effect of the relative humidity over the photocatalytic reaction suggests a negative effect of adsorbed water on the formaldehyde sorption capacity, similar to what was observed for toluene on the same systems. The competition of water molecules for the active sites and saturation of smaller pores becomes the dominant effect reducing the efficiency of photocatalytic oxidation of both hydrophobic (toluene) and hydrophilic (formaldehyde) pollutants.

3.2.2. *Effect of the UV light source*

Table 2 summarizes HCHO photocatalytic removal rates determined under different humidity and irradiation conditions. Fig. 4 shows HCHO removal efficiency for a sub-set of those results corresponding to experiments performed at 10% RH under UVA, UVC and UVC/O_3 irradiation. The use of a UVA lamp led to lower removal efficiency, principally due to the significantly lower irradiance of the UVA source used with respect to the UVC lamps. Instead, the UVC/O_3 source showed in most cases higher removal efficiencies than the ozone-free UVC lamp, even if its irradiance at 254 was ~60% lower than that of the ozone-free UVC lamp. This is likely due to the added effect of ozone chemistry and direct photolysis under 254 + 185 nm irradiation [15,19,20]. It is worth noting that, while removal rates per unit mass of TiO_2 ($F_r/m_{f\text{-}TiO_2}$) values reported in Table 2 for hecto-TiO_2 were in most cases below those reported for P25 under the same conditions, the use of the UVC/O_3 lamp led to a better performance for hecto-TiO_2 composites relative to P25 under either dry air or moderate humidity conditions (10% RH). This result suggests that the clay matrix serves as a substrate that facilitates the secondary chemical processes present under 254 + 185 nm irradiation. This effect may be due, at least in part, to the higher surface area and uptake capacity of the clay, which allows for more HCHO to be exposed to the reactive conditions under UVC/O_3 irradiation.

3.2.3. *Effect of the reactor residence time*

By increasing the airflow rate and reducing the length of the reactor we explored the performance of the reaction at different residence times under 10% RH and UVA irradiation. The results are illustrated in Fig. 5, for the range of residence times was between 50 and 500 ms. As expected, the net removal efficiency decreased as the residence time decreased, consistent with our previous observations using the same reactor [16]. We did not observe

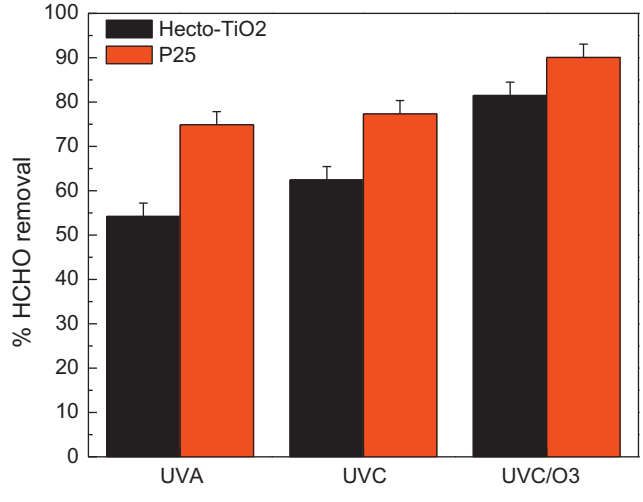

Fig. 4. Effect of UV source on HCHO photocatalytic removal at 10% RH.

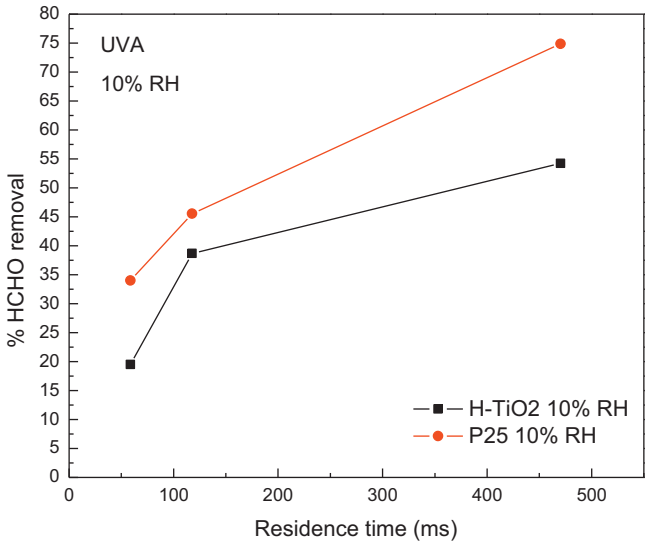

Fig. 5. Effect of the reactor residence time on HCHO removal efficiency.

any significant difference on the relative ratio hecto-TiO_2/P25 of removal efficiencies determined for each residence time. Hecto-TiO_2 was consistently below P25, with a %*R* that was between 60% and 80% that of P25.

4. Conclusions and implications

We evaluated the performance of hectorite-TiO_2 nanocomposites with respect to the reference material P25 under controlled conditions of relative humidity, UV irradiation and residence time, using formaldehyde as a target compound. Overall, the clay-TiO_2 composite showed comparable efficiency in the removal of the model pollutant when normalized by the mass content of TiO_2. The observed influence of key experimental parameters on clay-TiO_2 is consistent with that observed on P25 and with previously reported mechanisms for formaldehyde photocatalytic oxidation [21,22]:

$$TiO_2 \xrightarrow{h\nu} e^- + h^+ \quad (5)$$

$$HCHO + H_2O + 2h^+ \rightarrow HCOOH + 2H^+ \quad (6)$$

$$HCOOH + 2h^+ \rightarrow CO_2 + 2H^+ \quad (7)$$

$$O_2 + 4e^- + 4H^+ \rightarrow 2H_2O \quad (8)$$

These results support the use of clay-TiO_2 composites as pollution-removing active ingredients in the formulation of paints, coatings, pavement and cement [23–26]. Potential benefits of incorporating TiO_2 nanoparticles in the clay matrix include higher durability, slower inactivation, and avoiding leaching of nanoparticles to the environment. These results complement those reported previously using toluene as a target compound [15], allowing us to characterize the clay-TiO_2 photocatalyst by challenging it with model hydrophobic and hydrophilic organic pollutants that are relevant to indoor environments and atmospheric chemistry.

Acknowledgments

This work was supported by Laboratory Directed Research and Development (LDRD Project #08-103, LB07014) funding from Lawrence Berkeley National Laboratory, provided by the Director, Office of Science, of the U.S. Department of Energy under Contract No. DE-AC02-05CH11231. J.C.S. thanks B.Sc. Cesar Saavedra Alamillas, M. in Sc. María del Rocío Galindo Ortega (Universidad Autónoma Metropolitana Unidad Cuajimalpa), M. in Sc. Pilar Fernández Lomelin (Instituto de Geografía, UNAM) for technical assistance, and ECACORE 2020 (SEMARNAT-CONACYT) for financial assistance. We express gratitude to M. Trejo (UNAM) for his participation in the synthesis of composite materials, and to L. Charlet, A. Fernandez-Martinez and M.C. Leroy for helpful discussions.

References

[1] A.T. Hodgson, D. Beal, J.E.R. McIlyaine., Sources of formaldehyde, other aldehydes and terpenes in a new manufactured house, Indoor Air 12 (2002) 235–242.
[2] B.C. Singer, H. Destaillats, A.T. Hodgson, W.W. Nazaroff, Cleaning products and air fresheners: emissions and resulting concentrations of glycol ethers and terpenoids, Indoor Air 16 (2006) 179–191.
[3] H. Destaillats, M.M. Lunden, B.C. Singer, B.K. Coleman, A.T. Hodgson, C.J. Weschler, W.W. Nazaroff, Indoor secondary pollutants from household product emissions in the presence of ozone. A bench scale study, Environ. Sci. Technol. 40 (2006) 4421–4428.
[4] M.J. Mendell, Indoor residential chemical emission as risk factors for respiratory and allergic effects in children: a review, Indoor Air 17 (2007) 259–277.
[5] K. Pazdrak, P. Gorski, A. Krakowiak, U. Ruta, Changes in nasal lavage fluid due to formaldehyde inhalation, Int. Arch. Occup. Environ. Health 64 (1993) 515–519.
[6] M.J. Mendell, W.J. Fisk, K. Kreiss, H. Levin, D. Alexander, W.S. Cain, J.R. Girman, C.J. Hines, P.A. Jensen, D.K. Milton, L.P. Rexroat, K.M. Wallingford, Improving the health of workers in indoor environments: priority research needs for a national occupational research agenda, Am. J. Pub. Health 92 (2002) 1430–1440.
[7] V.J. Cogliano, Y. Grosse, R.A. Baan, K. Straif, M.B. Secretan, F. El Ghissassi, Meeting report: summary of IARC monographs on formaldehyde, 2-butoxyethanol and 1-tert-butoxy-2-propanol, Environ. Health Perspect. 113 (2005) 1205–1208.
[8] W.J. Fisk, 2008, http://eetd.lbl.gov/ied/sfrb/voc-sensory.html.
[9] EEA, Impacts of Europe's Changing Climate, OPOCE (Office for Official Publications of the European Communities), European Environment Agency, 2004, http://reports.eea.eu.int/climate_report_2_2004/en.
[10] K. Civerolo, C. Hogrefe, B. Lynn, J. Rosenthal, J.Y. Ku, W. Solecki, J. Cox, C. Small, C. Rseonszweig, R. Goldberg, K. Knowlton, P. Kinney, Estimating the effects of increased urbanization on surface meteorology and ozone concentrations in the New York City metropolitan region, Atmos. Environ. 41 (2007) 1803–1818.
[11] A.T. Hodgson, H. Destaillats, D. Sullivan, W.J. Fisk, Performance of ultraviolet photocatalytic oxidation for indoor air cleaning applications, Indoor Air 17 (2007) 305–316.
[12] A.T. Hodgson, H. Destaillats, T. Hotchi, W.J. Fisk, Evaluation of a combined ultraviolet photocatalytic oxidation (UVPCO)/chemisorbent air cleaner for indoor air applications. Report prepared to the Building Technologies Program of the U.S. Department of Energy, Contract No. DE-AC02-05CH11231 [LBNL-62202], 2007.
[13] M. Sleiman, P. Conchon, C. Ferronato, J.M. Chovelon, Photocatalytic oxidation of toluene at indoor air levels (ppbv): towards a better assessment of conversion, reaction intermediates and mineralization, Appl. Catal. B: Environ. 86 (2009) 159–165.
[14] D. Kibanova, M. Trejo, H. Destaillats, J. Cervini-Silva., Synthesis of hectorite-TiO_2 and kaolinite–TiO_2 nanocomposites with photocatalytic activity for the degradation of model air pollutants, Appl. Clay Sci. 42 (2009) 563–568.
[15] D. Kibanova, J. Cervini-Silva, H. Destaillats, Efficiency of clay-TiO_2 nanocomposites on the photocatalytic elimination of a model hydrophobic air pollutant, Environ. Sci. Technol. 43 (2009) 1500–1506.
[16] N. Quici, M.L. Vera, H. Choi, G. Li Puma, D.D. Dionysiou, M.I. Litter, H. Destaillats, Effect of key parameters on the photocatalytic oxidation of toluene at low concentrations in air under 254 + 185 nm UV irradiation, Appl. Catal. B: Environ. 95 (2010) 312–319.
[17] I. Pengelly, J.A. Groves, J.O. Levin, R. Lindahl, An investigation into the differences in composition of formaldehyde atmospheres generated from different source materials and the consequences for diffusive sampling, Ann. Occup. Hyg. 40 (1996) 555–567.
[18] USEPA, Compendium Method TO-11A – Determination of Formaldehyde in Ambient Air Using Adsorbent Cartridge Followed by HPLC [Active Sampling Methodology], Office of Research and Development-US Environmental Protection Agency, Cincinnati, OH, 1999.
[19] J. Jeong, K. Sekiguchi, W. Lee, K. Sakamoto, Photodegradation of gaseous volatile organic compounds (VOCs) using TiO_2 photoirradiated by an ozone-producing UV lamp: decomposition characteristics, identification of by-products and water-soluble organic intermediates, J. Photochem. Photobiol. A 169 (2005) 279–287.
[20] J. Jeong, K. Sekiguchi, K. Sakamoto, Photochemical and photocatalytic degradation of gaseous toluene using short-wavelength UV irradiation with TiO_2 catalyst: comparison of three UV sources, Chemosphere 57 (2004) 663–671.
[21] C. Passalia, M.E. Martinez Retamar, O.M. Alfano, R.J. Brandi, Photocatalytic degradation of formaldehyde in gas phase on TiO_2 films: a kinetic study, Int. J. Chem. Reactor Eng. 8 (2010) A161.
[22] J. Peral, D.F. Ollis, Heterogeneous photocatalytic oxidation of gas-phase organics for air purification: acetone, 1-butanol, butyraldehyde, formaldehyde and m-xylene oxidation, J. Catal. 136 (2) (1992) 554–565.
[23] V. Matejka, P. Kovar, P. Babkova, J. Prikryl, K. Mamulova-Kutlakova, Utilization of photoactive kaolinite/TiO_2 composite in cement-based building materials,

in: Z. Bitnar, et al. (Eds.), Nanotechnology in Construction – Part 3, Springer, 2009, pp. 309–314.
[24] A. Strini, S. Cassese, L. Schiavi, Measurement of benzene, toluene, ethylbenzene and o-xylene gas phase photodegradation by titanium dioxide dispersed in cementitious materials using a mixed flow reactor, Appl. Catal. B: Environ. 61 (2005) 90–97.
[25] C. Aguia, J. Angelo, L.M. Madeira, A. Mendes, Photo-oxidation of NO using an exterior paint – screening of various commercial titania in powder pressed and paint films, J. Environ. Manage. 92 (2011) 1724–1732.
[26] M.M. Ballari, M. Hunger, G. Husken, H.J.H. Brouwers, NO_x photocatalytic degradation employing concrete pavement containing titanium dioxide, Appl. Catal. B: Environ. 95 (2010) 245–254.